Heliyon 11 (2025) e42450

Contents lists available at ScienceDirect

Heliyon

journal homepage: www.cell.com/heliyon

Research article

Clofarabine-loaded aptamer-conjugated biodegradable nanoparticle successfully targeted CD117 overexpressed HL60 cells and potentially induced apoptosis

Manisheeta Ray [a,c], Ashique Al Hoque [a], Saptarshi Chatterjee [b], Sourav Adhikary [c], Samrat Paul [b], Biswajit Mukherjee [a,*], Amitava Bhattacharya [a]

[a] Department of Pharmaceutical Technology, Jadavpur University, 188, Raja S. C. Mullick Road, Jadavpur, Kolkata 700032, India
[b] BIRAC E-Yuva Centre, Adamas University, Adamas Knowledge City, Barackpore Main Rd, Barbaria, Kolkata, West Bengal 700126, India
[c] School of Materials Science and Nanotechnology, Jadavpur University, Kolkata, India

ARTICLE INFO

Keywords:
Acute myeloid leukemia (AML)
DNA aptamer
Targeted delivery
Nanoparticles
Biomarker CD117

ABSTRACT

Acute Myeloid Leukemia (AML) is a rapidly progressing malignancy characterized by the proliferation of abnormal neutrophils, leading to severe symptoms and complications. Current widely used treatment options include chemotherapy and radiotherapy, which often result in suffering from systemic toxicity and drug resistance. To mitigate systemic toxicity and off-target side effects, a targeted therapeutic strategy is one of the remarkably successful options. For targeting AML cells, we have chosen a single-strand DNA aptamer (Apt), which is specific for the biomarker CD117, overexpressing AML cells. This study introduces explicitly a novel therapeutic approach employing aptamer-conjugated clofarabine-loaded PLGA nanoparticles (Apt-CNP) targeting the CD117 receptor on HL60 leukemia cells. Clofarabine, a potent nucleoside analogue, disrupts DNA synthesis and induces cancer cell death but is limited by its toxicity and resistance. Encapsulation in PLGA nanoparticles enables sustained drug release, maintaining therapeutic concentrations and potentially reducing drug resistance. Our findings demonstrate that Apt-CNP effectively targets HL60 leukemia cells, thereby improving drug delivery and reducing adverse effects on healthy cells. This targeted approach may open a new avenue for more specific drug delivery to mobile and floated blood cells, including AML (HL60 leukemia) cells, and overcome the limitations of traditional AML treatments.

1. Introduction

Acute myeloid leukemia (AML) is a bone marrow and blood malignancy characterized by the rapid growth of abnormal myeloblasts, precursors of granulocytes, which also hinder the production of healthy red blood cells [1]. Symptoms include weakness, fatigue, fever, easy bruising or bleeding, and recurrent infections. Treatment options include radiation, chemotherapy, stem cell transplantation, and targeted therapy based on patient health, age, and leukemia cell characteristics [2].

Clofarabine, a nucleoside analogue, inhibits ribonucleotide reductase, disrupting DNA synthesis and causing death to cancer cells, although leading to toxicity to normal healthy cells, too [3,4]. Clinical trials highlight clofarabine's efficacy against leukemia but also

* Corresponding author.
E-mail addresses: biswajit.mukherjee@jadavpuruniversity.in, biswajit55@yahoo.com (B. Mukherjee).

https://doi.org/10.1016/j.heliyon.2025.e42450
Received 31 January 2025; Accepted 3 February 2025
Available online 4 February 2025

note limitations such as drug resistance and toxicity [5]. Targeted nanocarrier therapy, using drug-loaded biodegradable (The United States Food and Drug Administration (US-FDA) approved polymer) poly (lactic-co-glycolic acid) (PLGA) nanoparticles, through systemic administration can enhance drug delivery and minimize adverse effects [6–8].

Ligand-conjugated delivery, involving ligands like antibodies and aptamers, offers precise targeting of cells, including AML cells, enhancing therapeutic efficacy and reducing toxicity [9]. Aptamers (also called synthetic monoclonal antibodies) are stable, cost-effective, less immunogenic compounds to monoclonal antibodies, highly target-specific, and ideal for targeted drug delivery [10, 11].

This study introduces aptamer-conjugated clofarabine-loaded PLGA nanoparticles (Apt-CNP) targeting the CD117 (c-KIT) overexpressed receptor on the cell surface of the majority of AML cells, including HL60 AML cells. This approach aims to minimize adverse effects by specifically delivering clofarabine to leukemia cells, enhancing treatment efficacy, and reducing systemic toxicity [9]. PLGA nanoparticles ensure sustained drug release and prolonged blood levels, which would potentially reduce drug resistance [7].

The novelty of this work lies in the development of Apt-CNP as a targeted drug delivery system for floated acute myeloid leukemia cells. The hypothesis driving this study is that conjugating a CD117-specific aptamer to clofarabine-loaded PLGA nanoparticles will significantly enhance the therapeutic efficacy of clofarabine by selectively targeting AML cells, such as HL60 while reducing systemic toxicity and minimizing off-target effects. This novel approach combines the target specificity of aptamers with the sustained drug release capabilities of PLGA nanoparticles, addressing limitations like drug resistance and adverse effects associated with conventional AML therapies.

2. Experimental

2.1. Materials

Clofarabine was procured from TCI Chemicals India Pvt Ltd, Telangana. PLGA (MW 4,000–15,000; lactide to glycolide ratio 75:25) was sourced from Sigma-Aldrich Chemicals Pvt. Ltd., Bangalore. Polyvinyl alcohol (PVA, MW 125,000) was purchased from S.D. Fine-Chem Ltd., Mumbai. Fluorescein isothiocyanate (FITC) was obtained from Himedia Lab Pvt. Ltd., Mumbai. Acetone, acetonitrile, and dichloromethane (DCM) were procured from E. Merck (India) Ltd., Mumbai. All other chemicals were analytical grade, ensuring high purity.

HL60 cells were procured from National Centre for Cell Science (NCCS), Pune.

U937 cells were procured from Dr. Amitava Sengupta, Senior Principal Scientist and Associate Professor of biological sciences, CSIR, Indian Institute of Chemical Biology (IICB-TRUE).

PBMC were isolated from anticoagulated blood (blood with anticoagulant).

2.2. Selection of aptamer

We selected a single-stranded DNA aptamer specific for the CD117 biomarker [12]. The DNA aptamer sequence was 5′-GAGGCATACCAGCTTATTATTGGGGCCGGGGCAAGGGGGGGGTACCGTGGTAGGACAGATAGTAAGTGCAATCTGCGAA-3′ with K_d value of 4.24 nM, indicating a strong affinity between the aptamer and its target molecule [9].

2.3. Method

.

2.4. Preparation of clofarabine encapsulated PLGA nanoparticles (CNP)

PLGA nanoparticles were synthesized using a modified multiple-emulsion solvent evaporation method [13,14]. PLGA with a 75:25 lactic acid to glycolic acid ratio (50 mg) was dissolved in 3 mL of a dichloromethane (DCM) and acetone mixture (1:1 v/v). PVA solutions were prepared at 1.5 % and 2.5 % (w/v) by dissolving PVA in Milli-Q water with continuous stirring and heating at 50 °C. Clofarabine (5 mg), the drug of interest, was added to the 2.5 % PVA solution to create a drug-loaded aqueous phase. The emulsification process was initiated by homogenizing the PLGA organic solution into 2.5 % PVA solution at 6000 rpm for 3 min using an Ultra-Turrax homogenizer (IKA Laboratory Equipment, Germany), forming a primary water-in-oil (W/O) emulsion. This primary emulsion was added to 1.5 % PVA solution and homogenized for 8 min to create a water-in-oil-in-water (W/O/W) double emulsion. To improve particle stability and reduce droplet size, the secondary emulsion was then sonicated for 30 min and stirred overnight. Large particles and aggregates were separated by an initial centrifugation step at 5000 rpm, ensuring that only fine particles remained in the supernatant. This supernatant was centrifuged at 16,000 rpm for 45 min to isolate the nanoparticles. To remove residual PVA, the nanoparticle pellet was washed three times by resuspending it in deionized water, followed by repeated centrifugation at 16,000 rpm for 10 min each. The nanoparticles were then pre-freezed at −20 °C for 9 h to prevent aggregation and structural compromise and lyophilized for 8 h using a freeze dryer (Instrumentation India, Kolkata, India) to obtain dry, stable nanoparticles for further characterization and applications. This method ensures efficient drug encapsulation and high nanoparticle stability, making it suitable for advanced drug delivery systems.

FITC-tagged nanoparticles were prepared following the same protocol as previously described. Specifically, 100 μl of a FITC solution in ethanol (0.4 % w/v) was added to the organic phase containing the polymer and drug before the homogenization step. All

subsequent procedures remained unchanged.

2.5. Drug-excipient interaction study using Fourier Transform Infrared spectroscopy (FTIR)

This study investigates potential interactions between clofarabine and various excipients utilizing Fourier Transform Infrared (FTIR) spectroscopy, a robust analytical technique to identify changes in chemical bonds and functional groups. FTIR spectroscopy is a critical tool for assessing chemical compatibility in pharmaceutical formulations. By comparing FTIR spectra of pure components, physical mixtures, and nanoparticles, any alterations or shifts in characteristic absorption bands indicate interactions. Pure clofarabine, PVA, PLGA, physical mixtures, drug-loaded nanoparticles, blank nanoparticles, and aptamer-conjugated nanoparticles were evaluated under an inert atmosphere using an FTIR spectrophotometer (Model: Prestige 22, Shimadzu, Japan) within the wave number range of 4000-400 cm^{-1}, using KBr pellets [15].

2.6. Analysis of aptamer and CD117 (c-KIT) interactions by molecular docking

For the molecular docking study, we selected CD117 (c-KIT), to which the aptamer can specifically bind in silico. The receptor's crystal structure (6GQJ) was retrieved from the RCSB (Research Collaboratory for Structural Bioinformatics) protein data bank (PDB) [16], and the DNA aptamer structure was created by adding the 79 base pair DNA sequence in Discovery Studio Visualizer 2021 and converting it to PDB format. The receptor was prepared by removing water molecules and adding polar hydrogen atoms and charges. The ligand molecule was also prepared for docking analysis using Discovery Studio Visualizer 2021. HDOCKlite blind docking software was used to examine interactions between the aptamer and tyrosine-protein kinase KIT protein [17]. The docking analysis and interactions were visualized through Biovia Discovery Studio 2021 (BIOVIA Discovery Studio - BIOVIA - Dassault Systèmes®, Vélizy-Villacoublay, France).

2.7. Aptamer conjugation on the surface of nanoparticles (Apt-CNP)

A 3′ amino and phosphorothioate backbone-modified aptamer was conjugated onto clofarabine-containing PLGA nanoparticle formulation using the well-established EDC/NHS method [18]. The clofarabine nanoparticle (CNP) was dissolved in deionized water at 5 mg/ml and incubated with 200 mM EDC and 100 mM NHS for 30 min at 25 °C. Excess EDC/NHS was removed by rinsing with DNase-RNase-free water. The aptamer, at 2.50 μM, was denatured and renatured by heating at 85 °C for 10 min and cooling for 10 min. This aptamer was combined with the activated CNP and reacted under rotation for 6 h. To ensure the purity of the resulting aptamer-CNP bioconjugates, the product was thoroughly washed with deionized water, effectively removing any unbound aptamer or residual reactants. This conjugation process yielded a stable and functional aptamer-nanoparticle complex suitable for further characterization and application in targeted drug delivery systems.

2.8. Agarose gel electrophoresis

Agarose gel electrophoresis offers a quick qualitative assessment of aptamer conjugation by observing shifts of aptamer in gel [16,19]. Compared to controls (non-conjugated nanoparticles and free aptamers), successful aptamer attachment to nanoparticles results in a shift. CNP conjugated with aptamer, aptamer non-conjugated nanoparticles and free aptamer were subjected to agarose gel electrophoresis. Samples included DNA ladder, Apt-CNP, free aptamer, and drug-loaded NP. The electrophoresis was run at 100V for 30 min with 0.5 mg/ml ethidium bromide to visualize base pairs (bp) on a 2 % agarose gel.

2.9. Drug loading and entrapment efficiency study

To evaluate % drug loading, 2 mg of the nanoformulation was mixed in 2 ml of acetonitrile and water (80:20) and incubated for 3–4 h in a shaker (Somax Incubator Shaker, China). Drug loading and entrapment efficiency were calculated as follows:

$$\text{Drug loading (Practical) (\%)} = \frac{\text{Quantity of drug present in nanoparticles} \times 100}{\text{Quantity of nanoparticles taken}}$$

$$\text{Entrapment efficiency (\%)} = \frac{\text{Practical drug loading} \times 100}{\text{Theoretical drug loading}}$$

2.10. Atomic force microscopy (AFM)

The atomic force microscopy (AFM) study provides detailed surface characterization at the nanometer scale. Samples were dissolved in Milli-Q water, vortexed, sonicated, cast on coverslips, and air-dried for 8 h. The transparent layer was visualized using AFM (5500 Agilent Technologies, USA) in tapping mode [20].

2.11. In vitro drug release study

In vitro drug release study indicates how drugs would be released from the particles in physiological conditions, providing a realistic assessment of how the drug-loaded nanoparticles could behave in the body [21]. The study was performed thrice using phosphate buffer saline (PBS) at pH 7.4 over 30 days. Accurately weighed nanoparticles were incubated in 2 ml PBS at 37° ± 0.5 °C in an incubator shaker. Pre-labeled samples taken at various intervals were centrifuged at 16,000 rpm for 30 min, and supernatants were analyzed at 263 nm [22] using UV–Vis spectroscopy.

The data from this study were plotted to test various kinetic models, namely, zero-order ($C = k_o t$), first-order ($\log C = \log C_o - k_1 t/2.303$), Higuchi ($Q = k\sqrt{t}$), and Korsmeyer-Peppas ($Mt/M\infty = Kt^n$) [23]. The zero-order model indicates drug release independent of drug concentration, promoting slow release. The first-order model shows the release rate linearly related to the remaining drug concentration. The Higuchi model explains drug release regulated by diffusion from a drug matrix. The Korsmeyer-Peppas model's "n" values characterize the release mechanism: $n \leq 0.45$ (Fickian diffusion), $0.45 < n < 0.89$ (non-Fickian diffusion), $n = 0.89$ (case II transport), and $n > 0.89$ (super case II transport) [24].

2.12. Particle size distribution and zeta potential

Particle size distribution and zeta potential analyses are crucial for nanoparticle characterization, providing insights into their physical and chemical properties [13]. Uniform particle size ensures consistent performance and stability, especially in drug delivery. Zeta Potential measured surface charge, indicating electrostatic repulsion between particles in their suspension. The average particle size and zeta potential of CNP and Apt-CNP were evaluated using a Malvern Zetasizer Nano-ZS 90 (Malvern Instruments, UK). Samples were dispersed in Milli-Q water, vortexed, and sonicated before analysis.

2.13. Field emissions scanning electron microscopy (FESEM)

Particle morphology was examined using a field emission scanning electron microscope, which offers ultra-high-resolution imaging in the nanometer range. This enables precise examination of surface morphology, particle size, shape, and distribution [25]. FESEM's lower accelerating voltages minimize the risk of damaging delicate nanoparticles, making it ideal for imaging soft materials and biological samples without compromising their integrity. The nanoformulation was deposited on carbon tape on a stub, coated with a 5 nm layer of platinum using a platinum coater, and visualized under a field emission scanning electron microscope (FESEM, JEOL JSM-7600F, Japan).

2.13.1. Stability study of the nanoparticles

In this study, we proceeded stability with the Apt-CNP only, as this was the formulation of our experimental interest. We have evaluated the particle surface morphology using FESEM of the Apt-CNP nanoformulation after storage at 4–8 °C in a refrigerator, and at 30 °C with 75 % relative humidity (RH) and at 40 °C with 75 % RH for 45 days, by particle size analysis for the samples stored at 30 °C and 40 °C, and FESEM analysis for all the three samples. Drug loading was also checked.

2.14. High-resolution Transmission electron microscopy (HR-TEM)

HR-TEM is an advanced imaging technique enables detailed visualization of the nanoparticle structure, providing critical perceptions into the internal morphology, surface characteristics, and the distribution of the encapsulated drug within the polymeric matrix. The HR-TEM analysis facilitated a deeper understanding of the structural integrity and homogeneity of the nanoparticle formulations, which are essential for evaluating their suitability for targeted drug delivery applications. HR-TEM was used to analyze internal morphology and drug distribution within the particles. Nanoparticles were suspended in Milli-Q water, dropped on a copper grid (300 mesh), and air-dried for 12 h. Samples were analyzed using HR-TEM (JEOL JEM 2100 HR, Tokyo, Japan) [15].

2.15. In vitro Cell cytotoxicity assay

AML cells, HL-60, were cultured under controlled conditions to maintain optimal growth and experimental reproducibility. The cells were supplemented with 10 % fetal bovine serum (FBS), 50 μg/ml streptomycin, and 50 IU/ml penicillin G in RPMI 1640 medium at 37 °C in a humidified incubator with a 5 % CO_2 atmosphere. Subculturing was performed every 72 h to ensure continuous exponential growth and cell viability. Similarly, Peripheral Blood Mononuclear Cells (PBMC) (PBMC were isolated from anticoagulated blood from human volunteers) and U937 cells were treated and analyzed under identical conditions in RPMI 1640. PBMC were isolated from anticoagulated blood. An equal volume of Ficoll-Hypaque was mixed with the anticoagulated blood and centrifuged at 400×*g* for 30 min [16]. The PBMCs were carefully collected from the interface between the two liquid layers, washed with PBS, and then resuspended in RPMI 1640 medium. Approximately $1.0–1.20 \times 10^4$ cells were cultured in 96-well plates with 100 μl RPMI 1640 media and incubated for 48 h with each formulation. After treatment, 20 μl MTT solution (5 mg/ml in PBS) was added and incubated for 4 h. Formazan crystals were dissolved in 100 μl DMSO, and optical densities were measured at 540 nm using an ELISA reader (Bio-Rad, CA, USA).

$$\text{Mean percentage viability} = \frac{\textit{Mean specific absorbance of treated cells} \times 100}{\textit{Mean specific absorbance of untreated cells}}$$

IC_{50} values were determined using OriginPro software, with experiments conducted in triplicate [15,26].

2.16. In vitro cellular uptake study

Cells were cultured under controlled conditions to maintain optimal growth and experimental reproducibility. This study provided the cellular uptake of drug-loaded nanoparticles (CNP) and aptamer-conjugated nanoparticles (Apt-CNP) by HL-60/U937 cells to evaluate the potential of targeted drug delivery. Since the formulations did not show cytotoxicity in PBMC in the experimental concentration range, the cell type was not considered for further study. Using flow cytometry, the internalization of fluorescent FITC-labeled nanoparticles was quantified. HL-60 cells treated with CNP and Apt-CNP were incubated for 12 and 24 h, collected by centrifugation, washed with ice-cold PBS, resuspended in PBS, and analyzed by a flow cytometer to measure nanoparticle uptake. U937 cells were cultured under the same conditions as HL-60 cells and treated with fluorescently labeled CNP and Apt-CNP for 24 h. After incubation, the cells were collected by centrifugation, washed with ice-cold PBS, resuspended in PBS, and analyzed by flow cytometry to evaluate nanoparticle uptake. The uptake results for U937 cells were used to compare the internalization efficiency between the two cell lines. Flow cytometry allows precise quantification of cellular internalization, providing crucial insights into the efficacy of targeted drug delivery [15,16,27].

2.17. Cellular apoptosis assay

The Annexin V FITC detects and quantifies apoptosis by tracking phosphatidylserine (PS) movement to the outer plasma membrane. Annexin V binds to PS and is labeled with FITC for fluorescence detection. HL60 cells (2.8×10^5/ml) were treated with IC_{50} concentrations of the free drug, CNP, and Apt-CNP for 24 h at 37 °C. Post-treatment, cells were centrifuged, counted to 10^5 in 100 μl of binding buffer, and incubated with 5 μl of Annexin V-FITC for 15 min in the dark. Cells were then diluted to 500 μl, 5 μl of propidium iodide was added, and they were analyzed using the FACS instrument with FITC (B530-A) and propidium iodide (YG586-A) channels. Similarly, U937 cells were treated and analyzed under identical conditions in RPMI 1640 to compare apoptosis induction between two cell lines. The data were presented in a four-quadrant plot to distinguish between live, early apoptotic, late apoptotic, and dead cells [28,29].

2.18. Mitochondrial membrane depolarization study by JC-1

Investigating mitochondrial membrane depolarization using JC-1 dye assesses changes in mitochondrial membrane potential [30]. JC-1 dye accumulates in mitochondria and exhibits potential-dependent fluorescence red at high membrane potential (J aggregates form) and green at low membrane potential (for monomers). During apoptosis, the mitochondrial membrane potential decreases, shifting from red to green fluorescence, indicating depolarization.

Apt-CNP was observed most effective in HL60 cells. Hence, HL60 cells were selected only for this investigation. HL60 cells (2.8×10^5/ml) were treated with IC_{50} concentrations of the free drug, CNP, and Apt-CNP for 24 h at 37 °C. After treatment, cells were washed with ice-cold PBS, incubated with JC-1 for 20 min, collected by centrifugation, and analyzed using FACS Diva software [16,31].

2.18.1. Statistical analysis

All the experiments were conducted in triplicate, and the data were presented as mean values with standard deviations. Statistical analysis was performed using one-way ANOVA and Student's t-test. Graphs and images were created using software tools like Origin 2021 and BIOVIA Discovery Studio Visualizer (BIOVIA—Dassault Systèmes®, Vélizy-Villacoublay, France). The graphical abstract was designed using Biorender.com.

3. Results

3.1. Drug-excipients interaction study by FTIR

FTIR studies were conducted to identify potential chemical interactions between the drug clofarabine and the excipients (PVA, PLGA) (Supplementary file: Figure S1 A). The analysis revealed distinct absorption peaks for PLGA at 3650 cm^{-1} (O–H stretching), 2935 cm^{-1} (asymmetric stretching of $–CH_2$), and 1735 cm^{-1} (C=O stretching of the carboxylic acid group). Pure clofarabine exhibited peaks at 3466.08 cm^{-1} (O-H stretching), 3113.19 cm^{-1} (N-H stretching), 1624.06 cm^{-1} (C=C stretching), 1581.62 cm^{-1} (C=N stretching), 1066.35 cm^{-1} (C-O stretching), 1244.08 cm^{-1} (C-N stretching), and 704.01 cm^{-1} (C-Cl stretching). The FTIR spectra of drug-loaded nanoparticles (CNP) and drug-loaded aptamer-conjugated nanoparticles (Apt-CNP) showed the characteristic peaks of clofarabine, indicating that the drug's chemical structure remained intact within these formulations. Additionally, new peaks corresponding to the constituting polymers were observed in the spectra of these nanoformulations, confirming their presence. Notably, the Apt-CNP exhibited a peak at 1635 cm^{-1}, signifying the binding of the aptamer to the nanoparticle surface through amide bond formation.

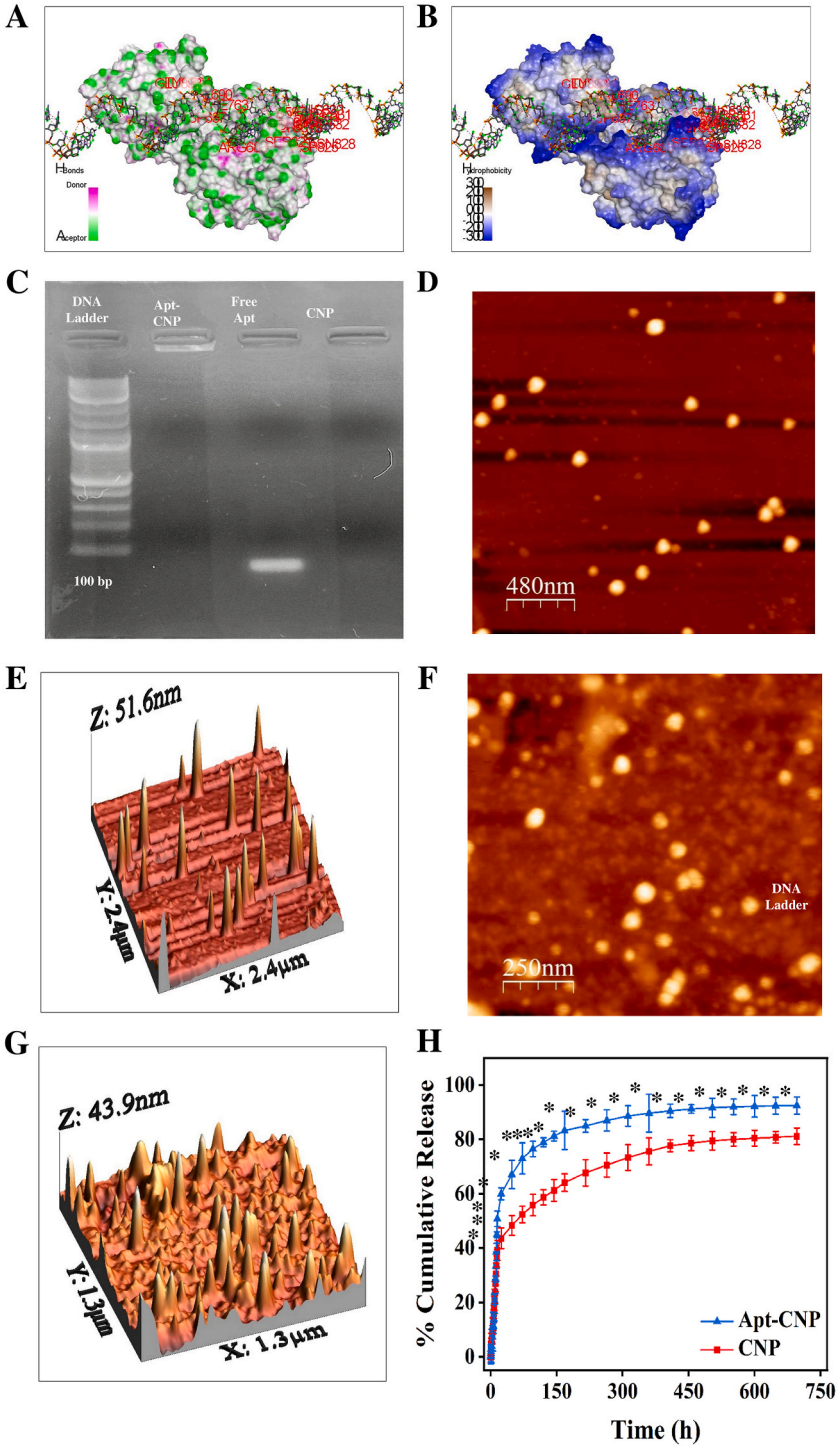

Fig. 1. Aptamer-tyrosine-protein kinase KIT, CD117 interactions by molecular docking, Aptamer conjugation with nanoparticles, In vitro drug release study, Atomic force microscopic evaluation of CNP and Apt-CNP (A) Aptamer-CD117 receptor interactions by hydrogen bonding through in silico molecular docking (B) Aptamer-CD117 receptor hydrophobic interactions through in silico molecular docking (C) Agarose gel electrophoresis confirming the conjugation of aptamer to the drug-loaded nanoparticle. (D), (E) AFM image of CNP. (F), (G) AFM image of Apt-CNP. (H) In vitro drug release of Apt-CNP and CNP. (data show mean ± SD, n = 3; * indicates $p < 0.05$ when compared with CNP treated group).

3.2. Analysis of aptamer-CD117 (c-KIT) interactions by molecular docking

A molecular docking study was conducted to assess the affinity and interactions between the 79 bp DNA aptamer and CD117 (c-KIT) protein. The results indicate that the nucleotide bases of the aptamer effectively bond with various amino acid residues (Fig. 1A and Fig. 1B). Various types of interactions (Table 1), including electrostatic, hydrophobic, and hydrogen bonding, were observed between different nucleotide bases of the DNA aptamer and different residue numbers such as guanine (DG 38), guanine (DG 39), guanine (DG 40), guanine (DG 41), guanine (DG 42), guanine (DG 43), adenine (DA 46), adenine (DA 47), cytosine (DC 48), guanine (DG 49), guanine (DG 50), guanine (DG 51), guanine (DG 57), guanine (DG 58), thymine (DT 59), and thymine (DT 60). These interactions occurred with various amino acid residues of the receptor protein, such as threonine (THR 594), leucine (LEU 595), glycine (GLY 596), alanine (ALA 597), glycine (GLY 598), alanine (ALA 599), lysine (LYS 626), histidine (HIS 630), serine (SER 631), threonine (THR 632), glutamic acid (GLU 633), arginine (ARG 634), asparagine (ASN 680), arginine (ARG 683), aspartic acid (ASP 816), lysine (LYS 818), asparagine (ASN 819), aspartic acid (ASP 820), serine (SER 821), aspartic acid (ASP 825), glycine (GLY 827), asparagine (ASN 828), alanine (ALA 829), arginine (ARG 686), aspartic acid (ASP 687), glutamic acid (GLU 688), phenylalanine (PHE 689), valine (VAL 690), proline (PRO 691), phenylalanine (PHE 763), glutamic acid (GLU 893), and tyrosine (TYR 894). The docking score revealed a value of −250.95, suggesting a strong binding affinity between the ligand and receptor.

3.3. Attachment of aptamer to the surface of nanoparticles

An agarose gel electrophoresis verified the attachment of CD-117 specific DNA aptamer to the nanoparticle surface. Fig. 1C shows that the 79-base pair aptamer migrated through the gel, aligning with the 100-bp marker on the conventional DNA ladder. In contrast, Apt-CNP remained in the loading well, as indicated by fluorescence. Notably, the unconjugated nanoparticles (CNP) did not produce any significant band in the well due to the absence of aptamer. For Apt-CNP, the image confirmed successful aptamer conjugation on the nanoparticle surface (Apt-CNP), supported by the earlier FTIR data, too.

3.4. Percentage of encapsulation efficiency and average drug loading of the formulation

The average drug loading of the CNP formulation was 23.63 ± 0.593 %, with an encapsulation efficiency of 70.92 %. The Apt-CNP mean drug loading was 21.78 ± 0.482 %, and the encapsulation efficiency was 69.86 %. Upon storing the formulations, Apt-CNP, at 4–8 °C in a refrigerator, and at 30 °C and 40 °C with 75 % relative humidity (RH) for 45 days did not vary drug loading significantly. Apt-CNP had drug loading 22.99 ± 0.671 % in the refrigerated condition, and the values of 21.27 ± 0.358 %. and 20.96 ± 0.432 % at 30 °C and 40 °C, respectively.

3.5. Atomic force microscopy (AFM)

We observed the atomic force microscopy imaging of CNP (Fig. 1D and Fig. 1E) and Apt-CNP (Fig. 1F and Fig. 1G). AFM images were acquired in both flattened topography and three-dimensional modes. The AFM data revealed that the conjugated nanoparticles maintained a spherical shape with a smooth surface.

3.6. In vitro drug release study

In vitro clofarabine release from CNP and Apt-CNP was conducted using phosphate buffer saline (PBS, pH 7.4) as it closely mimics the pH of human blood and extracellular fluid, facilitating a relevant environment to those in the human body [21]. The cumulative percentages of drug release for CNP and Apt-CNP were found to be 81.15 ± 3.036 and 92.45 ± 3.208, respectively, in 680 h of the study (Fig. 1H). The drug release data from the nanoparticles were evaluated using various kinetic models, including zero-order, first-order, Higuchi, and Korsmeyer–Peppas [32]. The regression coefficient (R^2) for each model and release exponent (n) values for the Korsmeyer–Peppas model were tabulated. The R^2 values (Table 2) indicate that drug release adhered to the Korsmeyer–Peppas model in the case of both formulations. In addition, the n-values suggested that the drug release followed the Fickian mechanism.

3.7. Measurement of particle size distribution and zeta potential and stability data of the nanoparticles

The zeta potential and particle size distribution were assessed using the dynamic light scattering method. The average hydrodynamic radius (dH) values for CNP and Apt-CNP were 154.7 nm and 175.2 nm, respectively (Fig. 2A). However, the aptamer conjugation resulted in an approximate 20 % increase in the size of the APT-CNP. The zeta potential values for CNP and Apt-CNP were −10.9 mV and −15.9 mV, respectively (Fig. 2B and Fig. 2C).

In this study, we proceeded with Apt-CNP only as it is the formulation of experimental interest and there has been no significant morphological change between the two formulations at 4–8 °C (Supplementary file: Figure S1 B). The formulations (Apt-CNP) stored at 30 °C and 40 °C with 75 % relative humidity (RH) (Fig. 2D and Fig. 2E) for 45 days exhibited enhancement of dH, and it might be due to particle agglomeration and deformation.

Table 1
Aptamer-CD117 (c-KIT) binding using molecular docking technique.

Name of the receptor	Protein Data Bank (PDB) code	DNA aptamer sequence	Docking score	Interacting residues	Interaction type
CD117 receptor, tyrosine-protein kinase KIT	6GQJ	5′-GAGGCATACC AGCTTATTATTGGGGCCGGGGCAAGGGGGGGGGTACCGTGGTAGGACAGATAGTAAGTGCAATCTGCGAA-3′	−250.95	THR 594, LEU 595, GLY 596, ALA 597, GLY 598, ALA 599, LYS 626, HIS 630, SER 631, THR 632, GLU 633, ARG 634, ASN 680, ARG 683, ASP 816, LYS 818, ASN 819, ASP 820, SER 821, ASP 825, GLY 827, ASN 828, ALA 829, ARG 686, ASP 687, GLU 688, PHE 689, VAL 690, PRO 691, PHE 763, GLU 893 and TYR 894.	electrostatic, hydrophobic interactions, hydrogen bonding

Table 2
Regression coefficient (R^2) values of in vitro drug release data employed in various kinetic models.

Kinetic Models	Formulations	
	CNP	Apt-CNP
Zero Order	$R^2 = 0.8594$	$R^2 = 0.7309$
First Order	$R^2 = 0.9309$	$R^2 = 0.8901$
Higuchi Model	$R^2 = 0.9554$	$R^2 = 0.8668$
Korsmeyer-Peppas Model	$R^2 = 0.9899$ $n = 0.2$	$R^2 = 0.9576$ $n = 0.12$

R^2 = regression coefficient and n = release exponent (slope of Korsmeyer-Peppas).

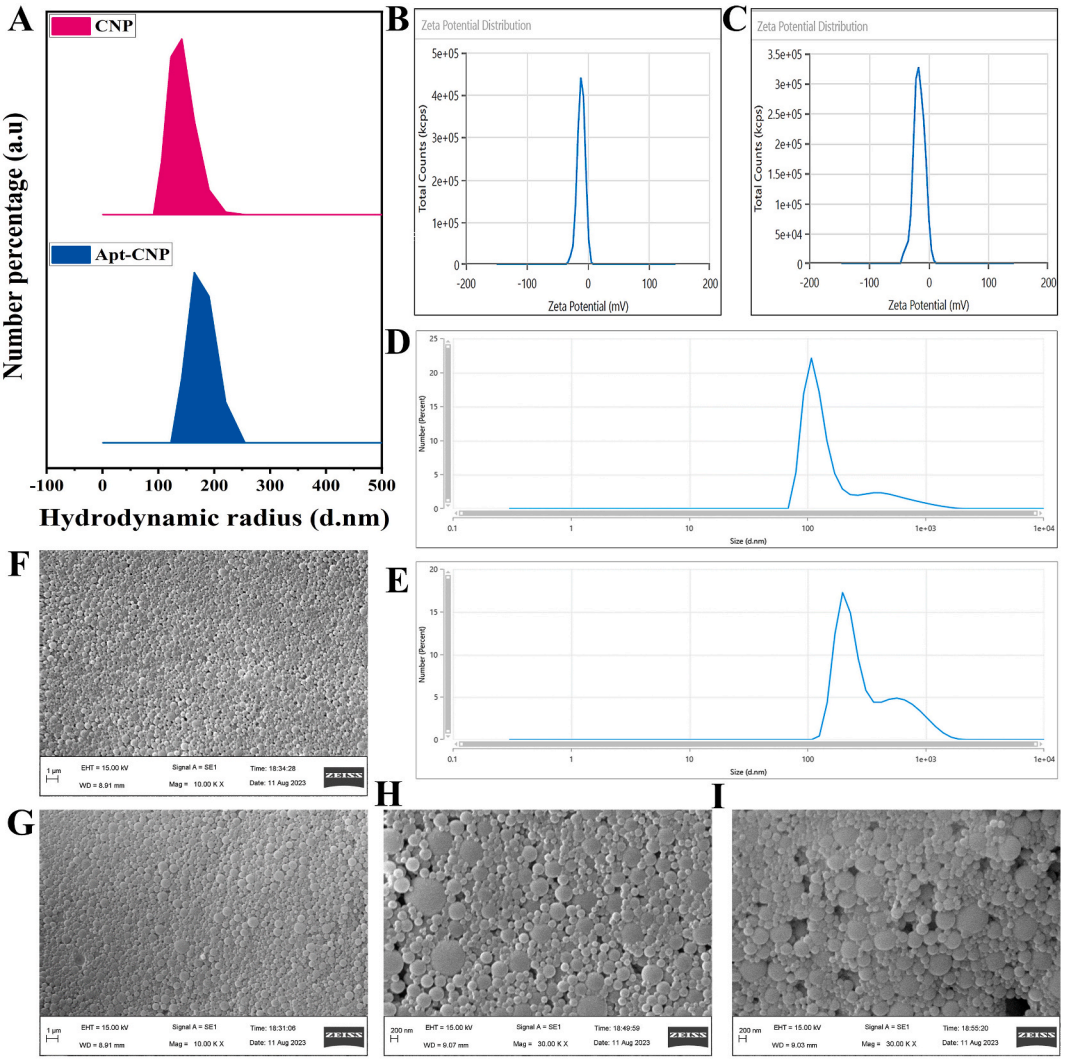

Fig. 2. Particle size and zeta potential of CNP and Apt-CNP, respectively, and stability-related particle size data of Apt-CNP stored at 30 °C and 40 °C with 75 % RH for 45 days, Electron microscopic imaging (FESEM) of CNP and Apt-CNP, Stability related FESEM of Apt-CNP stored at 30 °C with 75 % RH for 45 days. **(A)** Particle size of CNP and Apt-CNP. **(B), (C)** Zeta potential values of CNP and Apt-CNP, respectively. **(D)** Particle size distribution of Apt-CNP at 30 °C with 75 % RH for 45 days. **(E)** Particle size distribution of Apt-CNP at 40 °C with 75 % RH for 45 days. **(F)** FESEM image of freshly prepared CNP. **(G)** FESEM image of freshly prepared Apt-CNP. **(H)** FESEM image of Apt-CNP stored at 30 °C with 75 % RH for 45 days. **(I)** FESEM image of Apt-CNP stored at 40 °C with 75 % RH for 45 days.

3.8. Surface morphology of nanoparticle by field emissions scanning electron microscopy (FESEM)

FESEM analysis of the CNP and Apt-CNP nanoparticles demonstrated that both formulations exhibited smooth, spherical surfaces and closely distributed, with a mean hydrodynamic diameter of 100–250 nm, respectively (Fig. 2F and Fig. 2G). Aptamer-conjugation enhanced the size of the particles.

CNP and Apt-CNP stored at 30 °C and 40 °C with 75 % relative humidity (RH) for 45 days exhibited morphological changes with deformation and nanoparticle aggregation that might be due to polymer softening (Fig. 2H and Fig. 2I).

3.9. Internal morphology by transmission electron microscopy (HR-TEM)

We have studied the internal morphology of both CNP and Apt-CNP formulations through HR-TEM. Both the formulations revealed dark, spherical nanoparticles with a homogeneous internal structure (Supplementary file: Fig. S1 C and D), suggesting a homogenous distribution of the drug in the matrix.

3.10. Apt-CNP had variable IC_{50} values in HL60 and U937 cells, and non-toxic to Peripheral Blood Mononuclear Cells (PBMC)

The cell viability percentage of HL60 cells treated with clofarabine and experimental nanoparticles was evaluated using an MTT assay. Apt-CNP showed the highest toxicity to the HL60 cells (Fig. 3A) with the lowest IC_{50} value. The IC_{50} value of clofarabine was found to be 2.14 μM. The values were predominantly reduced in the nanoformulations, CNP, and Apt-CNP. The values were 1.30 μM and 1.07 μM in Hl60 cells, respectively, upon CNP and Apt-CNP treatments. In U937 cells, the IC_{50} values for clofarabine, CNP, and Apt-CNP were 2.31 μM, 1.81 μM, and 1.77 μM, respectively (Fig. 3B). When compared with HL60 cells, a similar trend is expected, but the extent of improvement with Apt-CNP may depend on the CD117 expression levels. The lack of significant enhancement in cytotoxicity with Apt-CNP compared to CNP suggests that the aptamer does not provide a targeting advantage in U937 cells, likely due to

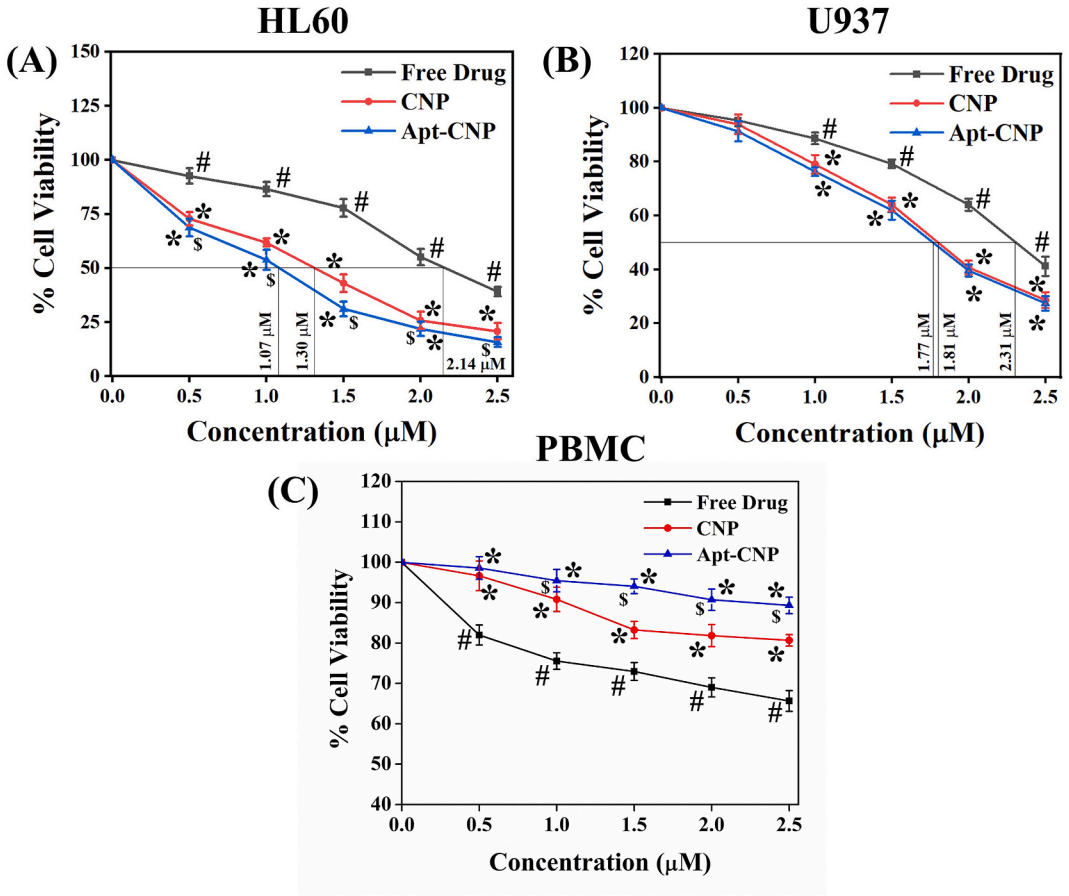

Fig. 3. In vitro cell cytotoxicity assay of the experimental nanoformulations on HL60 cells, U937 cells, and Peripheral Blood Mononuclear Cells (PBMC). **(A)** MTT assay data of the experimental nanoparticles on HL60 cells. **(B)** MTT assay data of the experimental nanoparticles on U937 cells. **(C)** MTT assay data of the experimental nanoparticles on PBMC cells (data show mean ± SD, n = 3; * indicates $p < 0.05$ when compared with the free drug-treated group, $ indicates $p < 0.05$ when compared with the CNP-treated group).

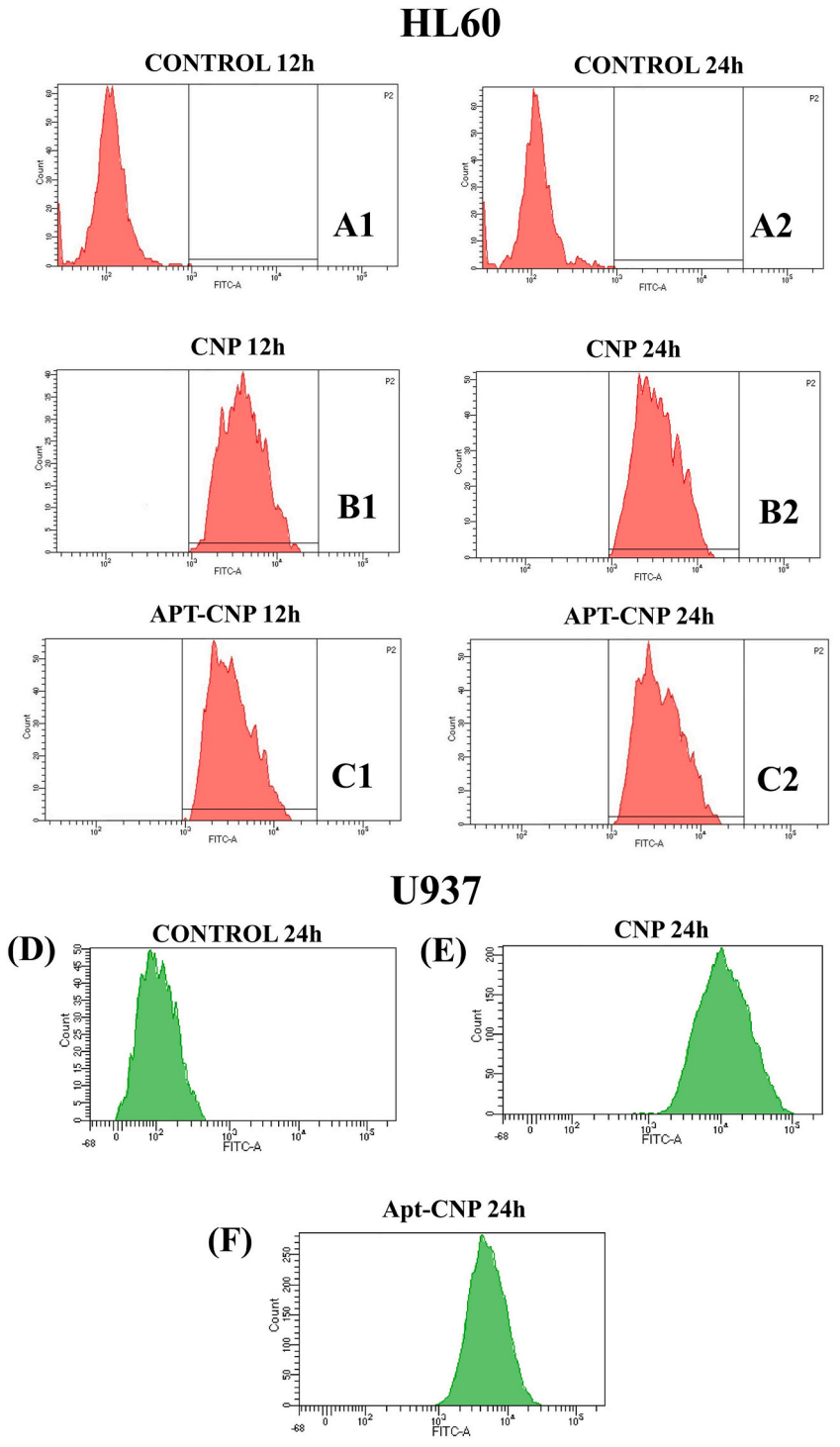

Fig. 4. In vitro HL60/U937 cellular uptake of the experimental formulations. **A1** and **A2** represent untreated control HL60 cells for 12 and 24 h, respectively. **B1** and **B2** represent CNP data for 12 and 24-h treatment, respectively. **C1** and **C2** represent data of Apt-CNP treatment for 12 and 24 h, respectively. **D** U937 control cells without treatment at 24 h. **E** U937 cells received CNP treatment for 24 h. **F** U937 cells received Apt-CNP treatment for 24 h.

the absence of the specific biomarker (CD117). In contrast, the cell viability assay conducted on normal cells (Peripheral Blood Mononuclear Cells, PBMC) did not yield IC_{50} values (Fig. 3C) for any of the formulations, suggesting minimal cytotoxicity and indicating a favorable safety profile of the formulations in non-cancerous cells.

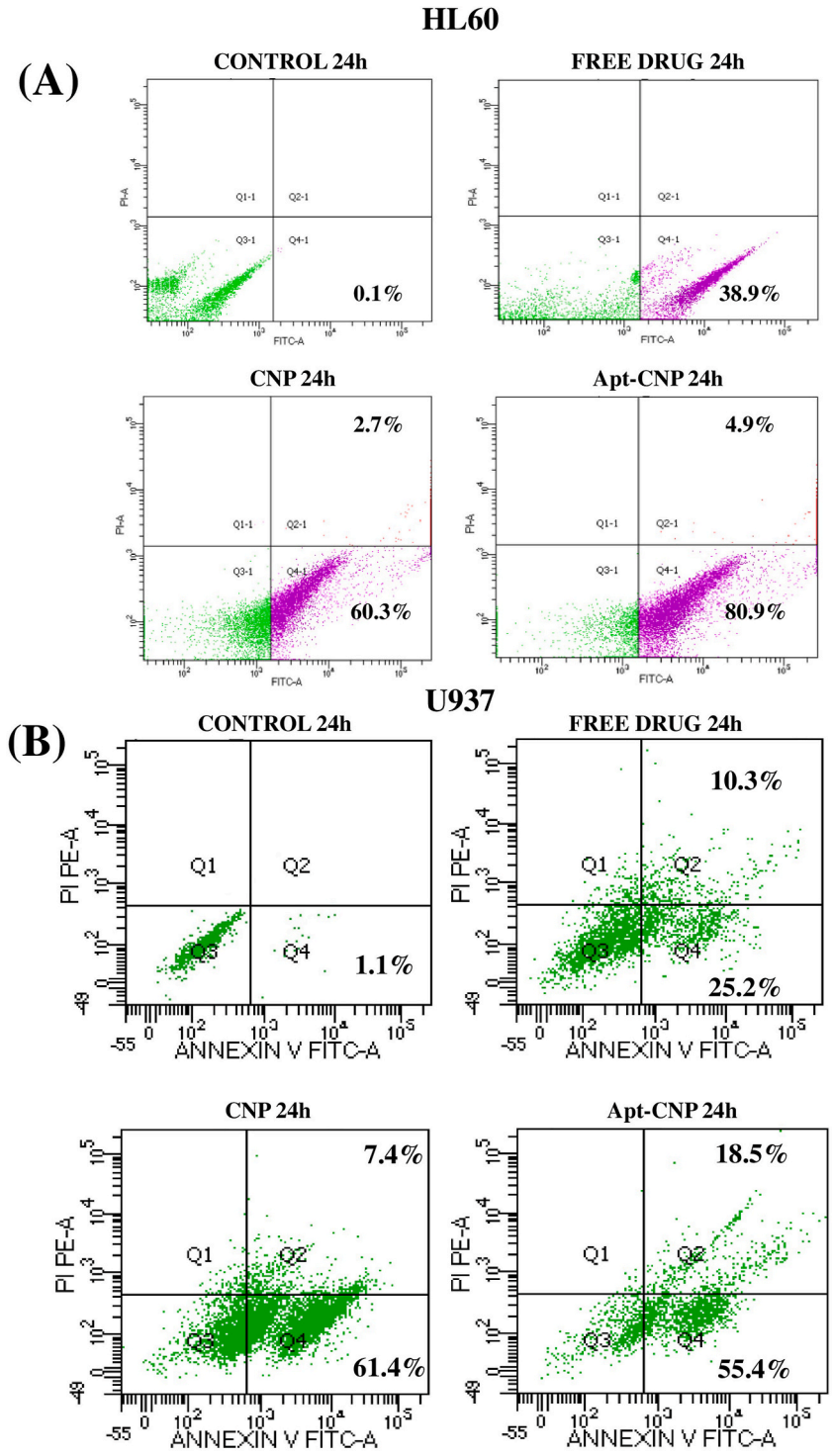

Fig. 5. Cellular apoptosis and cellular internalization of the experimental treatments on HL 60/U937 cells using flow cytometer. **(A)** In vitro cellular apoptosis study through Annexin V-FITC/PI on HL60 cells. **(B)** In vitro cellular apoptosis study through Annexin V-FITC/PI on U937 cells.

3.11. FITC-Apt-CNP showed maximum cellular internalization in vitro among the treatment groups

In vitro cellular uptake studies were conducted using flow cytometry to assess the internalization efficiency of FITC-labeled nanoformulations, CNP, and Apt-CNP in HL60 and U937 cells. HL60 is a human promyelocytic leukemia cell line extensively used in biomedical research, especially in studying hematopoiesis, myeloid leukemia, and cell differentiation [30]. These cells are known for their rapid proliferation in suspension culture. This rapid proliferation rate makes them an essential model for exploring the mechanisms of differentiation, apoptosis, drug resistance, and targeted drug delivery in leukemia research. U937, derived from human histiocytic lymphoma, is a widely recognized leukemia and monocytic differentiation study model [33]. Following treatment of HL60 cells with FITC-labeled CNP and Apt-CNP for 12 and 24 h, a significant enhancement in cellular uptake was observed with Apt-CNP compared to CNP. The analysis showed a substantial increase in cellular uptake for Apt-CNP formulations compared to nontreated control cells (Fig. 4 A1 and Fig. 4A2). The uptake of CNP reached 73.2 % (Fig. 4 B1), while Apt-CNP exhibited cellular uptake of 90.6 % (Fig. 4 C1) for 12 h. Again, in the case of 24 h, the uptake of CNP showed 82.9 % (Fig. 4B2), while Apt-CNP showed 95.6 % (Fig. 4C2). This marked increase in uptake for Apt-CNP compared to CNP highlights the significant role of the aptamer in enhancing the internalization of the nanoformulation in HL60 cells. Conversely, analysis in U937 cells showed 88.4 % uptake for CNP and 86.2 % for Apt-CNP (Fig. 4, D-F) after 24 h (though the difference of the data values were statistically non-significant) (Supplementary file: Fig. S2), indicating nonspecific uptake due to the absence of CD117 overexpression.

3.12. Apt-CNP treatment showed maximum cellular apoptosis in HL60 cells

The cellular apoptosis assay was performed using the Annexin V-FITC/PI dual staining method to evaluate the apoptosis-inducing potential of the free drug, CNP, and Apt-CNP in HL60 and U937 cells. After 24 h of treatment with free drug, CNP, and Apt-CNP, the early apoptotic populations in HL60 cells were 38.9 % early for free drug, 60.3 % for CNP, and 80.9 % for Apt-CNP. The late apoptosis in the Apt-CNP case was 4.4 %, the maximum among the treated groups (Fig. 5A). The results demonstrated a significant enhancement

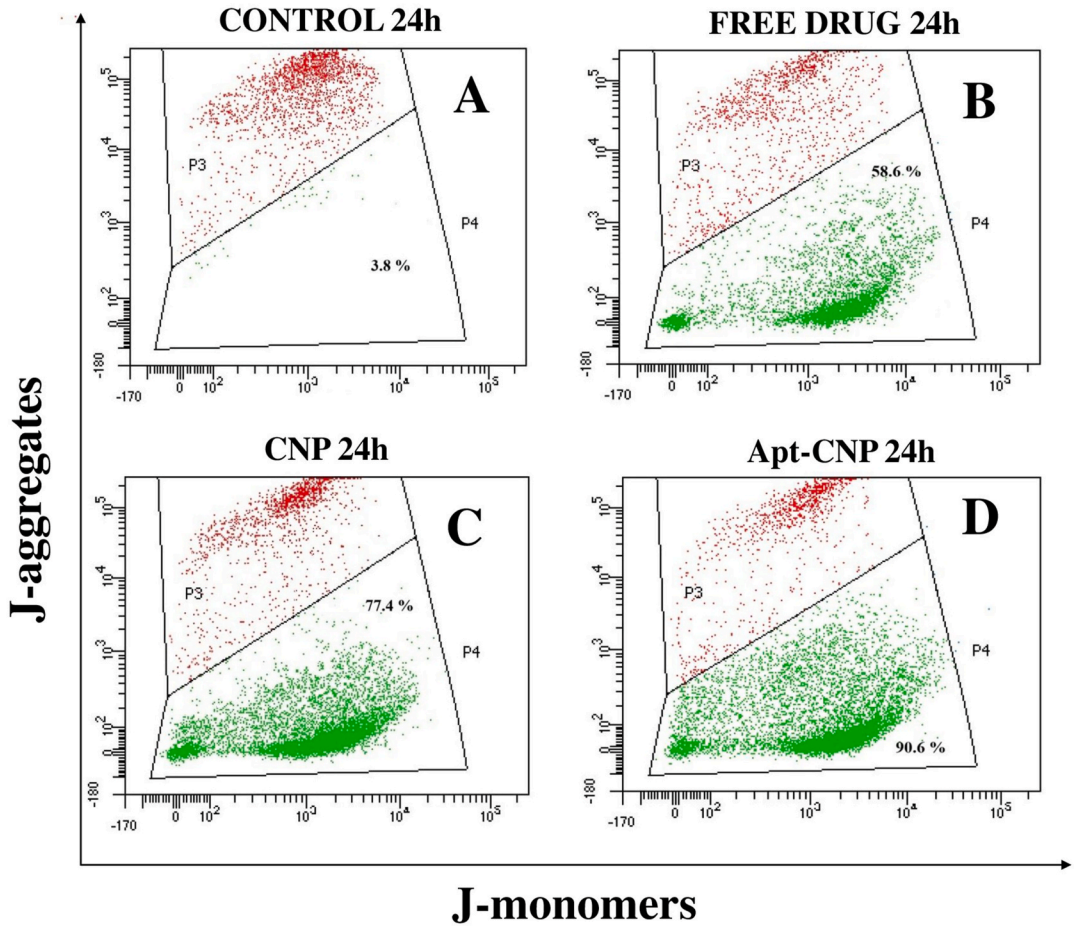

Fig. 6. Cellular mitochondrial membrane depolarization of HL60 cells, receiving experimental treatments using a flow cytometer. **A** Control **B** Free drug treatment for 24 h **C** CNP treatment for 24 h **D** Apt-CNP treatment for 24 h.

in apoptosis induction by Apt-CNP, highlighting its potential as an effective chemotherapeutic agent in HL60 cells. In contrast, U937 cells showed early and late apoptotic populations of 25.2 % and 10.3 % for the free drug, 61.4 % and 7.4 % for CNP, and 55.4 % and 18.5 % for Apt-CNP (Fig. 5B). Similar trends were expected, but the extent of apoptosis may vary depending on CD117 expression. These findings underscore the ability of Apt-CNP to selectively and efficiently induce apoptosis in CD117-positive leukemia cells (HL60), while minimizing off-target effects in non-target cells (U937), making it a promising candidate for targeted AML therapy.

3.13. Apt-CNP treatment predominantly enhanced mitochondrial membrane depolarization

Apt-CNP was found to be predominantly effective in HL60 cells compared to U937 cells. Hence, we have investigated effect of Apt-CNP on mitochondrial membrane polarization only in HL60 cells. The percentages of JC-1 monomer, which emitted green fluorescence, were 58.6 % for clofarabine, 77.4 % in the case of CNP, and 90.6 % for Apt-CNP after 24 h of treatment in HL60 cells (Fig. 6, A-D). The depolarized mitochondrial cell population predominantly increased for cells receiving Apt-CNP, clearly denoting its potency in higher apoptosis in HL60 cells. The data also correlate well with the cellular apoptosis data.

4. Discussion

We chose a biocompatible, biodegradable, US-FDA-approved polymer (PLGA) and a non-toxic, minimally immunogenic short nucleotide DNA aptamer [12,13]. This strategy aimed to ensure effective targeted drug delivery in vitro while reducing cytotoxicity to normal healthy cells due to less or no uptake of the targeted formultion. The approach focused on preferential accumulation of Apt-CNP in CD117 overexpressed AML cancer cells. HL60 cells were specifically chosen for this study due to their well-established use as a model for acute myeloid leukemia, providing a relevant and reliable system to assess the efficacy of the targeted delivery approach [26]. CD117 is overexpressed by about 70 % of AML varieties. They include HL60 cells. It is expressed in some normal cells too, although not overexpressed. Here, since a majority of AML variety overexpresses CD117, we have selected the protein as a target. Upon success of the formulation, this can work on the AML varieties those overexpress CD117. Secondly, this can be useful for targeting other expressed proteins on AML, by changing the protein specific aptamer.

Fourier-transform infrared (FTIR) spectroscopy was employed to investigate potential chemical interactions between the drug and the excipients [15], and the results indicate that no significant chemical interactions occurred between clofarabine and the excipients, ensuring the drug's stability and integrity within the nanoparticles. The stretching frequencies of the various functional groups of clofarabine-loaded nanoparticles (CNP) and aptamer-conjugated clofarabine-loaded nanoparticles (Apt-CNP) revealed the existence of the characteristic peaks of clofarabine, indicating that the drug's chemical structure remained unaltered in these formulations. Additionally, the spectra of these nanoformulations displayed drug peaks with the polymers, confirming drug incorporation. A peak at 1635 cm^{-1} in the Apt-CNP formulation signified the aptamer's attachment to the nanoparticle surface via amide bond formation. Therefore, the excipients used in the formulations are chemically compatible with the drug, making them suitable for drug delivery systems. The aptamer binding peak in Apt-CNP further validates the successful conjugation of the aptamer to the nanoparticles, which is crucial for targeted drug delivery applications.

The molecular docking study assessed the affinity and interactions between the DNA aptamer and CD117 (c-KIT), providing valuable insights into the binding dynamics and specificity of the aptamer. The findings indicate that the nucleotide bases of the aptamer formed strong bonds with various amino acid residues of the CD117 receptor. These interactions encompassed electrostatic, hydrophobic, and weak hydrogen bonding, underscoring the complexity and robustness of the binding mechanism. The amino acid residues involved in these interactions were not limited to the receptor's binding pocket but extended to other significant regions of the receptor, indicating a broad range of contact points between the aptamer and CD117. This extensive interaction network contributes to the aptamer's high binding affinity, as evidenced by the docking score of −250.95. Such a robust binding score suggests a highly stable complex, confirming the aptamer's potential for selective binding to the CD117 biomarker on AML cells (HL60). The selective binding of aptamer-conjugated nanoparticles to the CD117 receptor implies that these nanoparticles can effectively target AML cells, ensuring that the drug molecules are delivered directly to the cancer cells. This targeted delivery mechanism increases the drug concentration at the intended site and minimizes off-target effects, thereby enhancing the therapeutic index and reducing potential side effects [16].

Agarose gel electrophoresis was utilized to verify the attachment of the CD117-specific DNA aptamer to the nanoparticle surface. This method has confirmed the successful conjugation of the aptamer to nanoparticles [13]. The fluorescence observed in the Apt-CNP loading well confirms the DNA aptamer's presence on the heavier nanoparticle surface compared to the free aptamer. This finding is further supported by Fourier-transform infrared spectroscopy (FTIR) data, which provides additional evidence of the chemical bonds formed between the aptamer and the nanoparticles.

The average drug loading and percentage encapsulation efficiency results indicate that both formulations achieved substantial drug loading and good encapsulation efficiency, demonstrating their effectiveness in delivering the drug [21].

We have performed the in vitro drug release study of CNP and Apt-CNP using phosphate-buffered saline (PBS), pH 7.4, as a drug release medium. This setup ensures a relevant environment for studying the release of the drug in vitro under conditions similar to those in the human body [34]. Over 680 h, the cumulative drug release percentage from Apt-CNP was higher than that of CNP. Both the nanoparticles showed initial drug release followed by sustained drug release. Drug molecules near the surface might release the drug quicker initially, followed by sustained drug release from the core of the particles. The presence of aptamers on the surface of PLGA nanoparticles might reduce the binding affinity between the drug and the polymer matrix, facilitating comparatively faster drug diffusion out of the nanoparticles.

The FESEM analysis of CNP and Apt-CNP revealed that both types of nanoparticles displayed spherical and smooth surface

morphologies. The smooth surface appearance suggests that the synthesis and surface modification processes did not cause significant surface roughness or irregularities, which is often crucial for enhancing biocompatibility and reducing nonspecific interactions in biological environments [24]. The HR-TEM images demonstrated that the drug is present within the nanoparticles, confirming the uniformity of the internal morphology. The three-dimensional AFM images showed that the nanoparticles were well-separated and within a range of narrow size distribution. Additionally, these images confirmed the absence of pinholes on the nanoparticles.

The dynamic light scattering (DLS) technique was utilized to evaluate both the zeta potential and the particle size distribution of the nanoparticles. Analysis revealed an approximately 20 % size increase for aptamer-conjugated nanoparticles.

The zeta potential values provide insight into the stability of the nanoparticle suspensions. The negative values obtained suggest that both nanoparticle types possessed a moderate electrostatic repulsion that maintained their suspension in aqueous solutions over an extended period. As reported earlier, zeta potential values greater than ±30 mV are typically associated with highly stable suspensions due to stronger electrostatic repulsion [35]. Consequently, to ensure optimal stability and prevent aggregation, the nanoparticles should be stored in powder form at 2–8 °C (refrigerated condition) and suspended in water before injection.

The stability study of CNP and Apt-CNP revealed that samples stored at 4–8 °C retained their morphology and drug content consistently throughout the study. Conversely, samples stored at 30 °C with 75 % relative humidity (RH) and at 40 °C with 75 % RH for 30 and 45 days exhibited significant morphological alterations.

Higher temperatures induced morphological deformation and an increase in particle size due to polymer softening and nanoparticle aggregation. Stability was compromised at temperatures exceeding 30 °C, which underscores the necessity of maintaining storage temperatures between 2 and 8 °C (refrigerated) to preserve nanoparticle integrity [16,21].

After treating HL60 cells with FITC-labeled CNP and FITC-Apt-CNP for 12 and 24 h, the substantial increase of Apt-CNP uptake in HL60 leukemia cells compared to CNP treatment underscores the significant role of the aptamer in enhancing the internalization of the nanoformulation. The aptamer, designed to target the CD117 receptor on HL60 leukemia cells, effectively facilitated the targeted delivery and internalization of the nanoparticles. On the other hand, the significantly less uptake in U937 cells compared to HL60 cells highlights the specificity of the aptamer for CD117, a biomarker overexpressed in HL60 cells. Significantly less uptake in U937 cells was observed. This marked uptake data difference between HL60 and U937 cells confirms the specificity of aptamer-mediated targeting in CD117-overexpressing HL60 cells, emphasizing the potential of Apt-CNP for precise and effective drug delivery in CD117-overexpressing acute myeloid leukemia therapy. Compared to non-targeted CNP, these results underscore the enhanced efficacy of Apt-CNP in delivering the therapeutic formulation directly to CD117-overexpressed leukemia cells. Interestingly, floating, mobile neutrophils (HL60 cells) were very effectively targeted by Apt-CNP. It may be that the neutrophils which had a predominant role in phagocytosis could detect the Apt-CNP more effectively due to the binding of aptamer and the cell surface receptor CD117, and closed proximity might internalize more Apt-CNP in HL60 leukemia cells. This targeted approach improved the cellular uptake of the drug and potentially enhanced its therapeutic effects while minimizing off-target effects.

IC_{50}, or the half-maximal inhibitory concentration, is a crucial pharmacological indicator that quantifies the concentration of a substance required to inhibit a specific biological process or target by 50 %. In evaluating the cytotoxicity of a compound in cancer cells, a lower IC_{50} value indicates a greater potency. The MTT assay is the minimal amount of a substance necessary to achieve a 50 % reduction in cell viability or function, underscoring its efficacy at lower doses. Here, the MTT assay results highlight the superior therapeutic efficacy of Apt-CNP in HL60 cells, proving its potential as a targeted drug delivery system for CD117-overexpressing AML cells. The study investigated the effects of a free drug and experimental nanoparticles on the viability of HL60 cells, U937 cells, and normal PBMC cells. The Apt-CNP nanoparticles demonstrated the highest toxicity towards HL60 cells, with the lowest IC_{50} value. The IC_{50} was 1.30 μM for the CNP formulation, and for the Apt-CNP formulation, it was reduced to 1.07 μM in HL60 cells. In U937 cells, the absence of substantial improvement in cytotoxicity with Apt-CNP over CNP confirms the lack of specificity of the aptamer-mediated delivery system, to U937 cells, which lack CD117 expression. This reinforces the targeted nature of the formulation, which is tailored to exploit CD117 overexpression in HL60 cells. Moreover, the lack of cytotoxicity in PBMC cells underscores the safety profile of the nanoformulation, demonstrating its potential to minimize off-target effects and preserve normal cell viability [36]. This indicates that the nanoformulation, Apt-CNP, was more effective in reducing cell viability in HL60 cells and provides a promising strategy for selective AML therapy.

Apoptosis, the body's programmed cell death, is a crucial action for anticancer agents [37]. The apoptosis-inducing effects of clofarabine, CNP, and Apt-CNP were assessed here. The results emphasize the selective efficacy of Apt-CNP in inducing apoptosis in CD117-overexpressing HL60 cells. Apt-CNP was notably more effective in inducing apoptosis compared to clofarabine and CNP. The present findings highlight the superior apoptotic efficacy of Apt-CNP, with the highest proportion of cells undergoing early apoptosis and a notable percentage also progressing to late apoptosis. This suggests that Apt-CNP is highly effective in triggering apoptotic cell death in HL60 cells, reinforcing its potential as a potent chemotherapeutic agent with a strong cytotoxic impact. U937 cells lack CD117 overexpression and showed the absence of substantial enhancement in apoptotic induction by Apt-CNP compared to CNP. It further reinforces the specificity of the aptamer-mediated targeting mechanism. This selectivity improves therapeutic precision and minimizes off-target effects, a key requirement for effective cancer therapy. The enhanced apoptosis induction by Apt-CNP emphasizes its promising role in targeting CD117 receptors, making it a valuable candidate for further development and clinical testing in cancer therapy.

JC-1, a cationic dye, is a critical tool for evaluating alteration of mitochondrial membrane potential [38]. When JC-1 accumulates in mitochondria at high mitochondrial membrane potentials, it forms J-aggregates that emit red fluorescence. In contrast, depolarized or significantly less polarized mitochondria remain in their monomeric form in the cytosol, emitting green fluorescence [30]. Apt-CNP maximally depolarized mitochondrial membrane potential, leading to mitochondrial dysfunction and apoptosis in HL60 cells compared to free drug and CNP treatments. The enhanced mitochondrial depolarization observed with Apt-CNP underscores its

potential as a more effective therapeutic agent in inducing apoptosis [13], thus offering valuable insights for future therapeutic strategies targeting mitochondrial dysfunction in cancer cells.

Based on the data obtained from U937 cells, a clear pattern emerges, highlighting the nonspecific interaction of the formulations because of the absence of CD117 expression. While U937 cells showed some uptake of both CNP and Apt-CNP, as well as moderate cytotoxicity and apoptosis induction, the differences between these formulations are relatively minor. This lack of significant targeting for Apt-CNP in U937 cells accentuates the specificity of the aptamer for CD117-positive cells, such as HL60. Hence, no further study was conducted with U937 cells to investigate mitochondrial membrane potential. The lack of a JC-1 assay for U937 cells does not undermine the overall conclusions, as the current data clearly illustrate the selective targeting efficiency of Apt-CNP.

Due to constraints in experimental conditions, we could not explore the targeting of AML through in vivo experiments. It is worthwhile to investigate in vivo animal models such as xenograft techniques. Additionally, in vitro cell culture experiments can be enhanced by incorporating normal blood cells alongside AML cancer cells, providing a more comprehensive understanding of the targeted delivery to leukemic cells.

5. Conclusion

In conclusion, compared to non-conjugated formulations, CD117-specific aptamer conjugated clofarabine-loaded PLGA nanoparticles significantly improved cellular internalization in floated HL60 leukemia cells overexpressing CD117. This aptamer-nanoparticle formulation (Apt-CNP) enabled targeted drug delivery, resulting in superior in vitro therapeutic efficacy. These findings highlight the potential of aptamer-coupled nanoparticulate systems for targeted AML therapy. This novel nanoplatform not only showcases the significant potential for improving AML treatment outcomes but also opens avenues for developing targeted therapies for other hematologic malignancies. Further studies are warranted.

CRediT authorship contribution statement

Manisheeta Ray: Data curation, Formal analysis, Investigation, Methodology, Writing – original draft. **Ashique Al Hoque:** Software, Validation, Visualization, Writing – review & editing. **Saptarshi Chatterjee:** Investigation, Methodology. **Sourav Adhikary:** Software, Visualization. **Samrat Paul:** Data curation, Resources. **Biswajit Mukherjee:** Conceptualization, Funding acquisition, Project administration, Supervision, Visualization, Writing – review & editing. **Amitava Bhattacharya:** Resources, Supervision.

Funding

This study was supported by Dr. V. Ravichandran Center for Advanced Research in Pharmaceutical Sciences (CARPS), Jadavpur University. Grant no. CARPS/RA/01/2021. MR received the CARPS research fellowship.

Declaration of competing interest

The authors declare that they have no known competing financial interests or personal relationships that could have appeared to influence the work reported in this paper.

Acknowledgements

We also express our heartfelt gratitude to Dr. Amitava Sengupta, Senior Principal Scientist and Associate Professor of biological sciences, AcSIR, specializing in Cancer Biology and Inflammatory Disorders, for generously providing us with U937 cell line essential for our study.

Abbreviations:

CNP	Clofarabine nanoparticles
Apt-CNP	Aptamer conjugated clofarabine nanoparticles
PLGA	Poly (lactic-co-glycolic acid)
FESEM	Field Emission Scanning Electron Microscopy
HR-TEM	High-Resolution Transmission Electron Microscopy
FTIR	Fourier Transform Infrared Spectroscopy
AFM	Atomic Force Microscopy
FITC	Fluorescein isothiocyanate
PI	Propidium Iodide

Appendix A. Supplementary data

Supplementary data to this article can be found online at https://doi.org/10.1016/j.heliyon.2025.e42450.

References

[1] M.S. Shafat, B. Gnaneswaran, K.M. Bowles, S.A. Rushworth, The bone marrow microenvironment – home of the leukemic blasts, Blood, Rev. 31 (2017) 277–286, https://doi.org/10.1016/j.blre.2017.03.004.

[2] E.I. Obeagu, Q. Babar, Acute myeloid leukaemia (AML): the good, the bad, and the ugly. https://doi.org/10.22192/ijcrms.2021.07.07.004, 2021.

[3] W.B. Parker, V. Gandhi, Clofarabine: structure, mechanism of action, and clinical pharmacology, in: Chemotherapy for Leukemia: Novel Drugs and Treatment, Springer Singapore, 2017, pp. 261–286, https://doi.org/10.1007/978-981-10-3332-2_16.

[4] P.L. Bonate, L. Arthaud, W.R. Cantrell, K. Stephenson, J.A. Secrist, S. Weitman, Discovery and development of clofarabine: a nucleoside analogue for treating cancer, Nat. Rev. Drug Discov. 5 (2006) 855–863, https://doi.org/10.1038/nrd2055.

[5] M.J. Mauro, M.W. Deininger, Management of drug toxicities in chronic myeloid leukaemia, Best Pract. Res. Clin. Haematol. 22 (2009) 409–429, https://doi.org/10.1016/j.beha.2009.06.001.

[6] S. Correa, E.C. Dreaden, L. Gu, P.T. Hammond, Engineering nanolayered particles for modular drug delivery, J. Control. Release. 240 (2016) 364–386, https://doi.org/10.1016/j.jconrel.2016.01.040.

[7] F. Danhier, E. Ansorena, J.M. Silva, R. Coco, A. Le Breton, V. Préat, PLGA-based nanoparticles: an overview of biomedical applications, J. Control. Release. 161 (2012) 505–522, https://doi.org/10.1016/j.jconrel.2012.01.043.

[8] J.M. Anderson, M.S. Shive, Biodegradation and Biocompatibility of PLA and PLGA Microspheres, 1997.

[9] Y. Nur, S. Gaffar, Y.W. Hartati, T. Subroto, Applications of electrochemical biosensor of aptamers-based (APTASENSOR) for the detection of leukemia biomarker, Sens. Biosensing. Res. 32 (2021), https://doi.org/10.1016/j.sbsr.2021.100416.

[10] J. Zhou, J. Rossi, Aptamers as targeted therapeutics: current potential and challenges, Nat. Rev. Drug Discov. 16 (2017) 181–202, https://doi.org/10.1038/nrd.2016.199.

[11] A.D. Keefe, S. Pai, A. Ellington, Aptamers as therapeutics, Nat. Rev. Drug Discov. 9 (2010) 537–550, https://doi.org/10.1038/nrd3141.

[12] N. Zhao, S.N. Pei, J. Qi, Z. Zeng, S.P. Iyer, P. Lin, C.H. Tung, Y. Zu, Oligonucleotide aptamer-drug conjugates for targeted therapy of acute myeloid leukemia, Biomaterials 67 (2015) 42–51, https://doi.org/10.1016/j.biomaterials.2015.07.025.

[13] S. Chakraborty, Z.Y. Dlie, S. Chakraborty, S. Roy, B. Mukherjee, S.E. Besra, S. Dewanjee, A. Mukherjee, P.K. Ojha, V. Kumar, R. Sen, Aptamer-Functionalized drug nanocarrier improves hepatocellular carcinoma toward normal by targeting neoplastic hepatocytes, Mol. Ther. Nucleic Acids 20 (2020) 34–49, https://doi.org/10.1016/j.omtn.2020.01.034.

[14] M. Iqbal, N. Zafar, H. Fessi, A. Elaissari, Double emulsion solvent evaporation techniques used for drug encapsulation, Int. J. Pharm. 496 (2015) 173–190, https://doi.org/10.1016/j.ijpharm.2015.10.057.

[15] D. Dutta, A. Chakraborty, B. Mukherjee, S. Gupta, Aptamer-conjugated apigenin nanoparticles to target colorectal carcinoma: a promising safe alternative of colorectal cancer chemotherapy, ACS Appl. Bio Mater. 1 (2018) 1538–1556, https://doi.org/10.1021/acsabm.8b00441.

[16] A. Al Hoque, D. Dutta, B. Paul, L. Kumari, I. Ehsan, M. Dhara, B. Mukherjee, M. Quadir, B.A. Kaipparettu, S. Laha, S. Ganguly, ΔPSap4#5 surface-functionalized abiraterone-loaded nanoparticle successfully inhibits carcinogen-induced prostate cancer in mice: a mechanistic investigation, Cancer. Nanotechnol 14 (2023), https://doi.org/10.1186/s12645-023-00223-5.

[17] Y. Yan, H. Tao, J. He, S.Y. Huang, The HDOCK server for integrated protein–protein docking, Nat. Protoc. 15 (2020) 1829–1852, https://doi.org/10.1038/s41596-020-0312-x.

[18] O.C. Farokhzad, J. Cheng, B.A. Teply, I. Sherifi, S. Jon, P.W. Kantoff, J.P. Richie, R. Langer, Targeted nanoparticle-aptamer bioconjugates for cancer chemotherapy in vivo. www.pnas.orgcgidoi10.1073pnas.0601755103, 2006.

[19] M. Shahriari, S.M. Taghdisi, K. Abnous, M. Ramezani, M. Alibolandi, Self-targeted polymersomal co-formulation of doxorubicin, camptothecin and FOXM1 aptamer for efficient treatment of non-small cell lung cancer, J. Control. Release. 335 (2021) 369–388, https://doi.org/10.1016/j.jconrel.2021.05.039.

[20] Y. Herdiana, N. Wathoni, S. Shamsuddin, M. Muchtaridi, Drug release study of the chitosan-based nanoparticles, Heliyon 8 (2022) e08674, https://doi.org/10.1016/j.heliyon.2021.e08674.

[21] L. Kumari, I. Ehsan, A. Mondal, A. Al Hoque, B. Mukherjee, P. Choudhury, A. Sengupta, R. Sen, P. Ghosh, Cetuximab-conjugated PLGA nanoparticles as a prospective targeting therapeutics for non-small cell lung cancer, J. Drug, Target 31 (2023) 521–536, https://doi.org/10.1080/1061186X.2023.2199350.

[22] A. Shirman, Z.E. Inamdar, H.Y. Patel, N.S. Shaikh, A.I. Manyar, H.A. Siddiqi, A.S. Shaheena, Determination of clofarabine by uv visible spectrophometer and infra-red spectroscopy, Int. J. Biol. Pharm. Allied Sci. 9 (2020) 2085–2089. https://ijbpas.com/pdf/2020/August/MS_IJBPAS_2020_5131.pdf.

[23] G. Pattnaik, B. Sinha, B. Mukherjee, S. Ghosh, S. Basak, S. Mondal, T. Bera, Submicron-size biodegradable polymer-based didanosine particles for treating HIV at early stage: an *in vitro* study, J. Microencapsul. 29 (2012) 666–676, https://doi.org/10.3109/02652048.2012.680509.

[24] I. Ehsan, L. Kumari, R. Sen, A. Al Hoque, B. Mukherjee, A. Mukherjee, P. Ghosh, S. Bhattacharya, J591 functionalized paclitaxel-loaded PLGA nanoparticles successfully inhibited PSMA overexpressing LNCaP cells, J. Drug Deliv. Sci. Technol. 75 (2022) 103689, https://doi.org/10.1016/j.jddst.2022.103689.

[25] B.S. Satapathy, B. Mukherjee, R. Baishya, M.C. Debnath, N.S. Dey, R. Maji, Lipid nanocarrier-based transport of docetaxel across the blood brain barrier, RSC Adv. 6 (2016) 85261–85274, https://doi.org/10.1039/c6ra16426a.

[26] A. Aravind, S.H. Varghese, S. Veeranarayanan, A. Mathew, Y. Nagaoka, S. Iwai, T. Fukuda, T. Hasumura, Y. Yoshida, T. Maekawa, D.S. Kumar, Aptamer-labeled PLGA nanoparticles for targeting cancer cells, Cancer. Nanotechnol 3 (2012) 1–12, https://doi.org/10.1007/s12645-011-0024-6.

[27] E. Fathi, S. Azarbad, R. Farahzadi, S. Javanmardi, I. Vietor, Effect of rat bone marrow derived-mesenchymal stem cells on granulocyte differentiation of mononuclear cells as preclinical agent in cell based therapy, Curr. Gene Ther. 22 (2021) 152–161, https://doi.org/10.2174/1566523221666210519111933.

[28] N. Jan, A. Madni, M.A. Rahim, N.U. Khan, T. Jamshaid, A. Khan, A. Jabar, S. Khan, H. Shah, In vitro anti-leukemic assessment and sustained release behaviour of cytarabine loaded biodegradable polymer based nanoparticles, Life Sci. 267 (2021), https://doi.org/10.1016/j.lfs.2020.118971.

[29] R. Farahzadi, Z. Sanaat, A.A. Movassaghpour-Akbari, E. Fathi, S. Montazersaheb, Investigation of L-carnitine effects on CD44+ cancer stem cells from MDA-MB-231 breast cancer cell line as anticancer therapy, Regen. Ther. 24 (2023) 219–226, https://doi.org/10.1016/j.reth.2023.06.014.

[30] D. Dutta, A. Al Hoque, B. Paul, J.H. Park, C. Chowdhury, M. Quadir, S. Banerjee, A. Choudhury, S. Laha, N. Sepay, P. Boro, B.A. Kaipparettu, B. Mukherjee, EpCAM-targeted betulinic acid analogue nanotherapy improves therapeutic efficacy and induces anti-tumorigenic immune response in colorectal cancer tumor microenvironment, J. Biomed. Sci. 31 (2024), https://doi.org/10.1186/s12929-024-01069-8.

[31] J. Chen, X. Zhang, T. Singleton, F. Kiechle, Mitochondrial membrane potential change induced by Hoechst 33342 in myelogenous leukemia cell line HL-60, Ann. Clin. Lab. Sci. 34 (2004) 458–466.

[32] B. Sinha, B. Mukherjee, G. Pattnaik, Poly-lactide-co-glycolide nanoparticles containing voriconazole for pulmonary delivery: in vitro and in vivo study, Nanomedicine 9 (2013) 94–104, https://doi.org/10.1016/j.nano.2012.04.005.

[33] P. Harris, P. Ralph, Human leukemic models of myelomonocytic development: a review of the HL-60 and U937 cell lines, J. Leukoc. Biol. 37 (1985) 407–422, https://doi.org/10.1002/jlb.37.4.407.

[34] M. Dhara, A. Al Hoque, R. Sen, D. Dutta, B. Mukherjee, B. Paul, S. Laha, Phosphorothioated amino-AS1411 aptamer functionalized stealth nanoliposome accelerates bio-therapeutic threshold of apigenin in neoplastic rat liver: a mechanistic approach, J. Nanobiotechnology. 21 (2023), https://doi.org/10.1186/s12951-022-01764-4.

[35] J.A. Champion, Y.K. Katare, S. Mitragotri, Particle shape: a new design parameter for micro- and nanoscale drug delivery carriers, J. Control. Release. 121 (2007) 3–9, https://doi.org/10.1016/j.jconrel.2007.03.022.

[36] V.V. Veselov, A.E. Nosyrev, L. Jicsinszky, R.N. Alyautdin, G. Cravotto, Targeted delivery methods for anticancer drugs, Cancers 14 (2022) 622, https://doi.org/10.3390/cancers14030622.

[37] C. Yedjou, P. Tchounwou, J. Jenkins, R. McMurray, Basic mechanisms of arsenic trioxide (ATO)-induced apoptosis in human leukemia (HL-60) cells, J. Hematol. Oncol. 3 (2010) 28, https://doi.org/10.1186/1756-8722-3-28.

[38] A. Mathur, Y. Hong, B.K. Kemp, A.A. Barrientos, J.D. Erusalimsky, Evaluation of fluorescent dyes for the detection of mitochondrial membrane potential changes in cultured cardiomyocytes a a b c. www.elsevier.com/locate/cardioreswww.elsevier.nl/locate/cardiores, 2000.